Dust and gas obscuration in ELAIS Deep X-Ray Survey reddened quasars

Article (Published Version)

The Astrophysical Journal, 610:140–150, 2004 July 20

DUST AND GAS OBSCURATION IN ELAIS DEEP X-RAY SURVEY REDDENED QUASARS

Chris J. Willott,[1] Chris Simpson,[2] Omar Almaini,[3] Olivia Johnson,[3] Andrew Lawrence,[3] James S. Dunlop,[3] Nathan D. Roche,[3] Robert G. Mann,[3] James C. Manners,[4] Eduardo González-Solares,[5] Ismael Pérez-Fournon,[6] Rob J. Ivison,[7] Stephen Serjeant,[8] Seb J. Oliver,[9] Richard G. McMahon,[5] and Michael Rowan-Robinson[10]

Received 2004 February 4; accepted 2004 March 21

ABSTRACT

Hard X-ray surveys have uncovered a large population of heavily obscured AGNs. They also reveal a population of quasars with moderate obscuration at both visible and X-ray wavelengths. We use *Chandra*-selected samples of quasars from the ELAIS Deep X-ray Survey (EDXS) and the Chandra Deep Field–North to investigate the obscuration toward the nuclei of moderately obscured AGNs. We find an inverse correlation between the optical–to–X-ray flux ratio and the X-ray hardness ratio that can be interpreted as being due to obscuration at visible and X-ray wavelengths. We present detailed optical and near-infrared data for a sample of optically faint ($R > 23$) quasars from the EDXS. These are used to constrain the amount of rest-frame UV/optical reddening toward these quasars. It is found that optically faint quasars are mostly faint because of obscuration, not because they are intrinsically weak. After correcting for reddening, the optical magnitudes of most of these quasars are similar to the brighter quasars at these X-ray fluxes. Combining with gas column densities inferred from the X-ray observations, we consider the gas-to-dust ratios of the obscuring matter. We find that the quasars generally have higher gas-to-dust absorption than that seen in the Milky Way, similar to what has been found for nearby Seyfert galaxies. We consider the possible existence of a large population of X-ray sources that have optical properties of type 1 (unobscured) quasars but X-ray properties of type 2 (obscured) quasars. However, we find that such sources only contribute about 6% of the 0.5–8 keV X-ray background. Finally, we show that the observed distribution of optical–to–X-ray flux ratios of quasars at $z > 1$ is skewed to low values compared to the intrinsic distribution as a result of the fact that the observed-frame *R*-band light is emitted in the UV and is more easily obscured than hard X-rays.

Subject headings: galaxies: active — X-rays: galaxies

1. INTRODUCTION

The hard spectral shape of the X-ray background led to the idea that a large population of obscured active galactic nuclei (AGNs) exist that fail to show up in optically selected quasar surveys (Comastri et al. 1995). Deep hard X-ray surveys with *Chandra* and *XMM-Newton* have now revealed the sources responsible for the 0.5–10 keV X-ray background (e.g., Hornschemeier et al. 2001; Tozzi et al. 2001; Hasinger et al. 2001; Manners et al. 2003). As expected, the majority of the optical counterparts to hard X-ray sources are galaxies containing optically obscured AGNs.

Seyfert galaxies at low redshift often show complex absorption structures consisting of both cold (neutral) and warm (partially ionized) absorbers (Mushotzky et al. 1993). A fraction of Seyfert galaxies appear to be Compton thick and their observed X-ray emission is reflection dominated. Because of the low signal-to-noise ratio (S/N) of the X-ray spectra of the sources responsible for the X-ray background, there is only limited knowledge of their absorption properties. It is unknown whether the orientation-based obscuration scheme that works well for low-redshift Seyfert galaxies can also be applied at higher redshifts. There are still only a handful of type 2 narrow-line quasars found in deep X-ray surveys (Almaini et al. 1995; Norman et al. 2002; Stern et al. 2002; Crawford et al. 2002; Mainieri et al. 2002; Szokoly et al. 2004), seemingly at odds with simple unification schemes (however, there are still many faint objects without redshifts in these surveys that could be type 2 quasars). The relative lack of luminous type 2 quasars and the dominance of obscured AGNs at lower luminosities (Ueda et al. 2003; Hasinger et al. 2003) suggest that the fraction of obscured objects is a strong function of luminosity, as had previously been found for low radio frequency selected AGNs (Simpson et al. 1999; Willott et al. 2000). The fraction of Compton thick AGNs in the X-ray background sources is also quite uncertain (e.g., Fabian et al. 2002).

The dust properties of the high-redshift X-ray–absorbing material have not yet been well studied. There are certainly objects at low redshift with dust absorption quite different from that expected from the observed X-ray absorption based on a Galactic gas-to-dust ratio (Simpson 1998; Maiolino et al. 2001b), and a few cases of such discrepancies at higher redshifts have been reported (Akiyama et al. 2000; Risaliti et al.

[1] Herzberg Institute of Astrophysics, National Research Council, 5071 West Saanich Road, Victoria, BC V9E 2E7, Canada; chris.willott@nrc.ca.
[2] Department of Physics, University of Durham, South Road, Durham DH1 3LE, UK.
[3] Institute for Astronomy, University of Edinburgh, Royal Observatory, Blackford Hill, Edinburgh EH9 3HJ, UK.
[4] Dipartimento di Astronomia, dell'Universita di Padova, Vicolo dell'Osservatorio, 2-35122 Padova, Italy.
[5] Institute of Astronomy, University of Cambridge, Madingley Road, Cambridge CB3 0HA, UK.
[6] Instituto de Astrofísica de Canarias, Calle Vía Láctea s/n, 38200 La Laguna, Tenerife, Spain.
[7] UK Astronomy Technology Centre, Royal Observatory, Blackford Hill, Edinburgh, EH9 3HJ, UK.
[8] Centre for Astrophysics and Planetary Science, School of Physical Sciences, University of Kent, Canterbury, Kent CT2 7NZ, UK.
[9] Astronomy Centre, Department of Physics and Astronomy, University of Sussex, Falmer, Brighton BN1 9QH, UK.
[10] Astrophysics Group, Blackett Laboratory, Imperial College, Prince Consort Road, London SW7 2BW, UK.

2001; Willott et al. 2003; Watanabe et al. 2004). In this paper we discuss the dust and X-ray absorption present in hard X-ray sources contained within the ELAIS Deep X-ray Survey (EDXS) and the implications for understanding the sources responsible for the X-ray background.

In § 2 we discuss the observed correlations between optical and X-ray properties of X-ray–selected quasars and what these suggest about obscuration. In § 3 we present near-infrared and optical data for optically faint X-ray–selected quasars. In § 4 we fit model quasar spectra to the observations to constrain the reddening toward these quasars. In § 5 we compare the obscuration in the UV/optical with that in X-rays to determine the gas-to-dust ratio of the obscuring material and compare this with values in the Milky Way, the Small Magellanic Cloud, and low-redshift AGNs. In § 6 we discuss the effect that obscuration plays in altering the intrinsic optical–to–X-ray flux ratios of quasars to those observed. We assume throughout that $H_0 = 70$ km s^{-1} Mpc^{-1}, $\Omega_M = 0.3$, and $\Omega_\Lambda = 0.7$.

2. OPTICALLY FAINT QUASARS IN *CHANDRA* SURVEYS

In this paper we concentrate on X-ray sources that are associated with unresolved optical counterparts. With the exception of a few stars (readily identified by their high optical–to–X-ray flux ratios) these sources have optical and (usually) near-IR emission that is dominated by the active nucleus. We commonly refer to these objects as quasars for simplicity, but the reader should bear in mind that the moderate optical and X-ray luminosities place them around the border with type 1 Seyfert galaxies. It may seem strange that we decide to concentrate on quasars when galaxies dominate the hard X-ray background sources. However, quasars likely dominate the high-redshift, moderate-luminosity population (Barger et al. 2002; Hasinger et al. 2003; Steffen et al. 2003), and the presence of optical AGN continuum emission allows a more detailed investigation of the optical obscuration toward the nucleus, unlike the totally optically obscured X-ray sources associated with galaxies.

EDXS consists of two 75 ks *Chandra* pointings in northern ELAIS (European Large Area *ISO* Survey; Oliver et al. 2000) fields that have detected a total of 233 X-ray sources. Full details of the EDXS are given in Manners et al. (2003) and E. A. González-Solares et al. (2004, in preparation). In this paper we only consider sources in the EDXS-N2 region at R.A. = $16^{\rm h}36^{\rm m}47^{\rm s}$, decl. = $+41^\circ01'34''$ (J2000.0) because this region has superior optical imaging (seeing $0\farcs75$) that allows the separation of unresolved point sources and extended galaxies (which have typical sizes $\gtrsim 1''$) to a magnitude limit of $R = 25$. As seen below, classification at this magnitude limit is essential for identifying quasars at faint X-ray fluxes.

To increase the number of data points and therefore decrease statistical uncertainties in some of our analyses, we also use X-ray sources from the Chandra Deep Field–North (CDF-N) survey. The 1 Ms *Chandra* exposure detected 370 point sources (Brandt et al. 2001). Deep optical imaging of this field has been obtained and, crucially for our analyses, optically compact sources have been identified and flagged "C" for compact (Barger et al. 2002). Sources showing broad emission lines in their optical spectra are flagged "B" and sources both compact and with broad lines "BC." We include as quasars sources flagged as "BC" or "C" and also the four sources flagged "B" at redshifts $z > 0.8$ since the optical luminosities of these suggest that they are dominated by an AGN, and the fact that they were not classified as compact is likely due to the proximity of companions on the images.

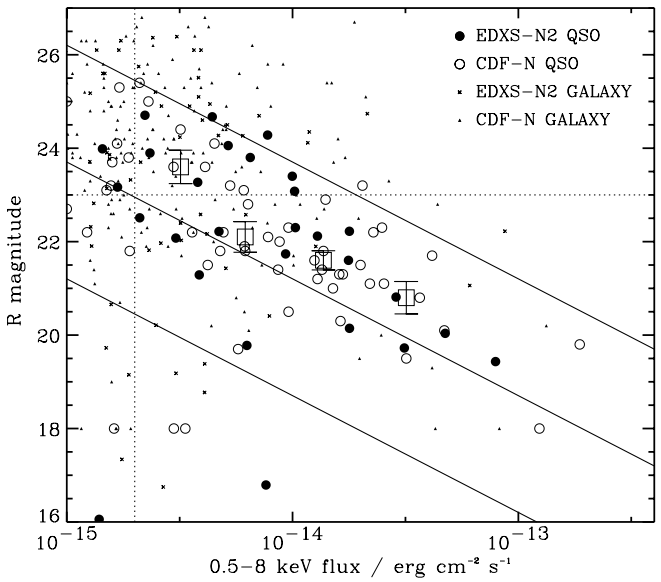

FIG. 1.—Optical magnitude vs. full-band X-ray flux for sources in the EDXS-N2 and CDF-N surveys. Quasars (as defined in § 2) are shown by circles. There is a well-known correlation between the optical and X-ray flux that is visible here for the quasars. The solid lines show constant optical–to–X-ray flux ratios of 0.1, 1, and 10 (*top to bottom*). The "quasars" with very high optical–to–X-ray flux ratios (>10) in the bottom left corner are stars. The vertical dotted line shows the X-ray flux limit considered throughout most of this paper. Quasars above this flux limit have been binned in X-ray flux, and the symbols with error bars show the median R magnitude against median X-ray flux in each bin with the associated standard error. The horizontal dotted line is at $R = 23$, and quasars above this line are classified as optically faint.

2.1. *Correlation between Optical and X-Ray Fluxes*

Figure 1 shows the R-band magnitude versus X-ray flux for X-ray sources from the EDXS-N2 and CDF-N surveys. Sources are shown as quasars if they are optically compact in EDXS-N2 or are quasars as defined above in the CDF-N. The vertical line shows a full-band (0.5–8 keV) flux limit of greater than 2×10^{-15} ergs cm^{-2} s^{-1}, which will be adopted for the remainder of this paper. This flux limit was chosen since it is equivalent to an S/N of 5 σ for most of the EDXS-N2 *Chandra* image. We use the full-band flux rather than just the hard-band (2–8 keV) flux since the energy-dependent response of *Chandra* is such that even moderately hard sources may be detectable in the full band, but not in the hard band. Note that at this flux limit a quasar with an optical–to–X-ray flux ratio (the ratio between the fluxes in the R band and the 0.5–8 keV band) of 0.1 has $R = 25.5$, close to the limiting magnitude at which one can separate unresolved from extended sources in ground-based optical imaging.

Figure 1 shows that the quasars tend to have a fairly small range of optical–to–X-ray flux ratio, as has been demonstrated before (Schmidt et al. 1998). There is some indication that the typical optical–to–X-ray flux ratio for quasars decreases at faint X-ray fluxes (in the faintest bin on Fig. 1), but this is not statistically significant. However, if there are significant numbers of $R > 25$ quasars that we have not identified as such, this difference and its significance could be increased. We investigate in this paper how this plot of optical and X-ray fluxes is affected by the existence of a sizeable number of partially obscured quasars.

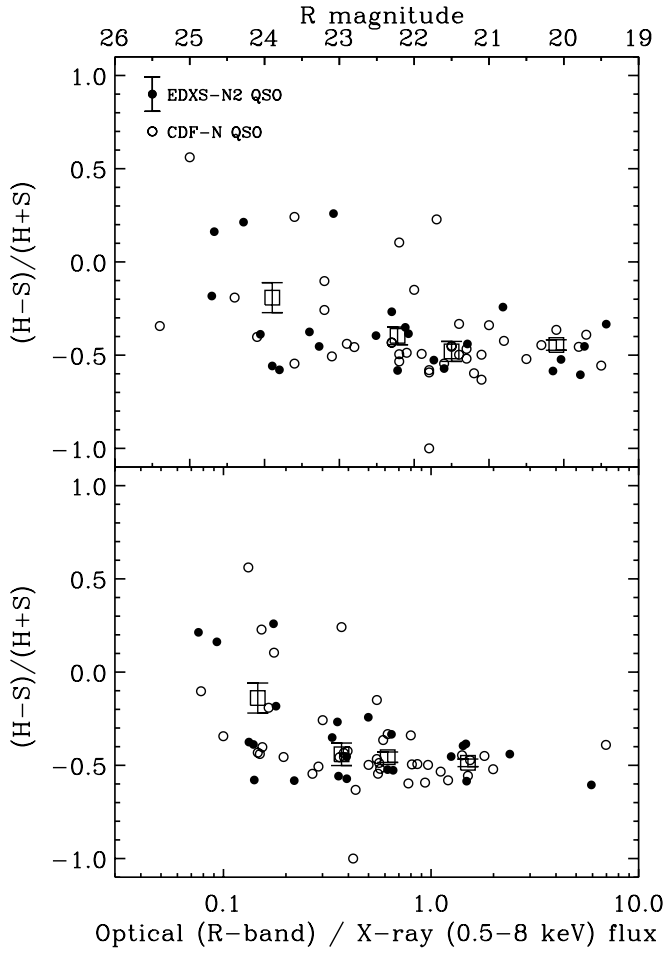

FIG. 2.—*Top*: Hardness of X-ray emission against *R*-band magnitude for quasars above a 0.5–8 keV flux limit of greater than 2×10^{-15} ergs cm^{-2} s^{-1} and with X-ray S/N greater than 5. The mean error bar on the hardness of these data is shown on the EDXS-N2 symbol label. The open squares show the mean hardness binned in optical magnitude and the associated standard error. *Bottom*: Hardness of X-ray emission against optical–to–X-ray flux ratio for the same quasars as in the top panel. The open squares show the mean hardness binned in optical–to–X-ray flux ratio and the associated standard error.

2.2. *The X-Ray Hardness Ratio and Optical and X-Ray Fluxes*

In order to determine whether obscuration may play a role in the observed optical–to–X-ray ratios, we now consider the hardness of the X-ray spectra of these sources as defined by $(H - S)/(H + S)$ (where H is the flux in the 2–8 keV band and S is the flux in the 0.5–2 keV band; see Manners et al. 2003 for more details). In the *XMM-Newton* survey of the Lockman Hole, Mainieri et al. (2002) showed that the full range of hardness values in surveys such as these can be explained by X-ray sources with a constant intrinsic power-law slope of $\Gamma \approx 2$ and a range of obscuring columns of 10^{19} cm$^{-2} < N_{\rm H} < 10^{24}$ cm^{-2}. Therefore, we use the observed hardness as an indicator of the gaseous obscuring column since the sources we discuss typically do not have enough counts for detailed spectral analyses. It should be remembered that a range of intrinsic power-law slopes could account for some of the scatter in observed hardness ratios.

Figure 2 shows the hardness ratio for quasars in the EDXS-N2 and CDF-N surveys plotted against *R*-band magnitude and optical–to–X-ray flux ratio. The binned data show some evidence that at faint optical magnitudes and at low optical–to–X-ray flux ratios, the typical hardness values of quasars increase, presumably because the X-ray emission becomes more heavily obscured. To test whether there are significant correlations, we perform a Spearman rank correlation analysis. The results show that there is a correlation between *R*-band magnitude and hardness significant at greater than 99% confidence and between optical–to–X-ray flux ratio and hardness at greater than 99.9%.

It is important to realize that the *R*-band magnitude is very strongly anticorrelated with the optical–to–X-ray flux ratio (>99.99999%) because most sources lie close to the X-ray flux limit. Hence, the appearance of both variables correlating with hardness could be induced by just one of the two being physically related to hardness. To ascertain if this is true, we employ a Spearman *partial* rank correlation analysis of the correlations present between the three variables. This method (e.g., Macklin 1982) assesses the statistical significance of correlations between the two named variables in the presence of the third. This analysis shows that the correlation between *R*-band magnitude and hardness (independent of correlations with optical–to–X-ray flux ratio) is only significant at 30% confidence. However, the correlation between optical–to–X-ray flux ratio and hardness (independent of correlations with *R*-band magnitude) is statistically significant at 98% confidence. Therefore, we find a significant increase in the X-ray obscuration of quasars at lower optical–to–X-ray flux ratios. Note that this correlation has the opposite trend from that expected if the optical and X-ray obscurations are completely independent.

This increase in X-ray obscuration of quasars at lower optical–to–X-ray flux ratios could be explained by an absorbing medium that contains dust and gas. At the typical redshifts of these quasars ($1 < z < 3$; see § 3), the observed *R*-band flux is probing the rest-frame UV and the observed 0.5–8 keV X-rays originate at harder energies. Therefore, the observed *R*-band flux is much more easily depressed than the X-ray flux. This idea is revisited in a more quantitative way in § 5. We need to first understand how much optical reddening there is in these quasars and then compare with the amount of X-ray absorption.

3. OBSERVATIONS

To understand the properties of quasars with low optical–to–X-ray flux ratios, we studied all those X-ray sources from the EDXS-N2 that have optically unresolved counterparts with $R > 23$, full-band fluxes greater than 2×10^{-15} ergs cm^{-2} s^{-1}, and *Chandra* S/N greater than 5. There are nine quasars obeying these criteria. Figure 1 shows that almost all these sources are located close to the optical–to–X-ray flux ratio = 0.1 line. One X-ray source, N2_25,[11] already has near-infrared and optical spectroscopy presented in Willott et al. (2003) and is found to be a quasar with fairly narrow emission lines (2000 km s^{-1}) subject to reddening of $A_V \approx 1$. In contrast to this fairly small amount of reddening, this quasar has a very hard X-ray spectrum indicating an obscuring column of $N_{\rm H} = 3 \times 10^{23}$ cm^{-2}.

3.1. *Near-Infrared Spectroscopy*

One source in the sample of nine $R > 23$ quasars, N2_35, has a particularly faint near-infrared counterpart ($K = 21$) and

[11] The full IAU name for this source is CXOEN2 J163655.7+405910. We use the abbreviated names of EDXS-N2 sources in this paper. Cross-referencing of the abbreviated and full names can be found in Manners et al. (2003).

TABLE 1
TABLE OF OBSERVED OBJECTS

SOURCE	NEAR-IR POSITION R.A.	NEAR-IR POSITION Decl.	z	0.5–8 keV FLUX (ergs cm^{-2} s^{-1})	HR	V MAGNITUDE	R MAGNITUDE	I MAGNITUDE	H MAGNITUDE
N2_15.....	16 37 04.40	+40 56 24.7	1.562	$(2.2 \pm 0.6) \times 10^{-15}$	-0.18 ± 0.23	25.35 ± 0.19	24.82 ± 0.10	24.13 ± 0.12	20.0 ± 0.2
N2_35[a]	16 36 49.28	+41 03 23.7	2.741	$(7.8 \pm 1.0) \times 10^{-15}$	0.16 ± 0.31	24.80 ± 0.09	24.72 ± 0.07	24.20 ± 0.10	...
N2_47.....	16 36 36.21	+41 05 09.2	0.884	$(3.8 \pm 0.7) \times 10^{-15}$	-0.45 ± 0.18	23.69 ± 0.10	23.43 ± 0.05	22.21 ± 0.05	20.2 ± 0.2
N2_60.....	16 36 19.18	+41 04 36.5	1.498	$(6.5 \pm 1.0) \times 10^{-15}$	-0.58 ± 0.13	24.35 ± 0.10	23.82 ± 0.05	23.04 ± 0.05	20.5 ± 0.2
N2_61.....	16 36 18.23	+41 00 37.4	1.390	$(5.2 \pm 0.9) \times 10^{-15}$	-0.39 ± 0.17	25.15 ± 0.14	24.08 ± 0.05	23.05 ± 0.05	20.3 ± 0.2
N2_64.....	16 36 14.45	+41 03 48.7	...	$(10.0 \pm 1.2) \times 10^{-15}$	-0.38 ± 0.11	23.30 ± 0.10	23.00 ± 0.05	22.24 ± 0.05	19.5 ± 0.2
N2_68[a]	16 37 25.33	+41 00 20.2	2.218	$(2.3 \pm 0.6) \times 10^{-15}$	-0.56 ± 0.11	24.15 ± 0.07	24.02 ± 0.05	23.49 ± 0.08	20.5 ± 0.2

NOTES.—Units of right ascension are hours, minutes, and seconds, and units of declination are degrees, arcminutes, and arcseconds. Shown are the EDXS-N2 optically faint quasars with near-infrared or optical spectroscopy presented in this paper. Hardness ratios are calculated by HR $= (H - S)/(H + S)$. Optical and near-IR magnitudes are measured in a 3″ aperture. N2_35 is not detected at H band but is detected at K with $K = 21.04 \pm 0.16$. The imaging data are described in E. A. González-Solares et al. (2004, in preparation), Roche et al. (2002), and Ivison et al. (2002).

[a] No near-infrared spectroscopy was obtained for these sources. Optical spectroscopy is described in § 3.2.

hence was not targeted since it was unlikely to yield a spectrum with sufficient S/N for analysis. The remaining seven quasars apart from N2_25 and N2_35 were the subject of a program of near-infrared spectroscopy with the OH Airglow Suppression Spectrograph (OHS; Iwamuro et al. 2001) on Subaru Telescope. The observations were carried out on the nights of UT 2002 May 20–24. Because of time constraints, we were only able to observe five of our targets. N2_37 and N2_68 were not observed. Optical spectra of N2_68 and N2_35 have been obtained instead (see § 3.2). The seven quasars that have data presented in this paper are listed in Table 1.

The OHS uses a fixed grism giving simultaneous J- and H-band spectra over the wavelength ranges 1.108–1.353 and 1.477–1.804 μm. The seeing was in the range 0.″5–0.″6 for all observations and a 0.″5 slit was used, giving a resolution of $\approx$40 Å (equivalent to 750 km s^{-1}). The total exposure times per object varied from 3200 to 7000 s depending on their near-IR magnitudes. These integrations were split into nodded frames of typically 1000 s each. Stars of spectral type F were observed immediately after each target to enable correction for atmospheric extinction.

The OHS data were reduced in a broadly standard manner, with extra care being taken to remove detector artifacts due to the faintness of our targets. Wavelength calibration was performed by observing the planetary nebula NGC 7027, while flux calibration and atmospheric extinction corrections were determined using the observations of HIP 80419. Further details can be found in Simpson et al. (2004). Photometric flux calibration was performed by scaling the reduced spectra by an aperture correction to account for slit losses. This calibration agrees well with the magnitudes from our own near-IR imaging (E. A. González-Solares et al. 2004, in preparation). The signal-to-noise ratios per resolution element (4 pixels) in H band for all the reduced spectra lie in the range 5–7.

3.2. *Optical Spectroscopy*

For two of the three $R > 23$ quasars for which we could not obtain near-infrared spectra, we have instead obtained optical spectra. N2_35 was observed with the Gemini Multi-Object Spectrograph (GMOS) at the Gemini North Telescope using nod-and-shuffle multiobject spectroscopy for a total of 3 hr. The data were reduced in a similar manner to that described in Abraham et al. (2004). N2_68 was observed in long-slit mode with the ISIS spectrograph at the William Herschel Telescope (WHT) in a similar manner to the observations described in Willott et al. (2003). An optical spectrum of N2_64 was also obtained with ISIS after the near-infrared spectrum failed to reveal a redshift.

3.3. *Redshifts*

The five OHS near-IR spectra are shown in Figure 3. Emission lines are detected in four of the five X-ray sources. Two sources (N2_15 and N2_60) have Hα λ6563 and [O III] λ5007 emission lines detected. The velocity offset of +700 km s^{-1} from Hα to [O III] in N2_15 is quite common in high-redshift quasars (McIntosh et al. 1999). In N2_47 there is one strong emission line that we identify as Hα and a probable detection of [S II] λ6716/λ6731 at the same redshift. N2_61 has just one secure emission line. We believe that this is Hα because of its high equivalent width and velocity width of 5000 km s^{-1} identifying it as a permitted line. There is a spike in the spectrum at the location of [O III] λ5007 for this redshift, but it is not definitely a real feature. N2_64 shows no emission lines in the OHS spectrum.

The optical spectrum of N2_68 showed a blue object with two strong, broad (2000–3000 km s^{-1}) emission lines. The wavelengths of these lines indicate that they are Lyα and C IV at a redshift of $z = 2.218$. A one-dimensional spectrum could only be extracted from the blue-arm data; there was insufficient signal in the red arm to locate the quasar. The spectrum is shown and used along with photometry in § 4 to constrain the amount of reddening of this quasar.

The optical spectrum of N2_35 has a blue continuum and several emission lines. The strongest emission line at 5790 Å has a deep absorption trough close to its center and what appears to be an absorption trough a few thousand kilometers per second blueward of the peak. Other weak, marginally significant emission lines are visible at 6139 and 7142 Å (these look more significant in the two-dimensional spectrum than in the one-dimensional spectrum). The locations of these emission lines give us a high degree of certainty that the redshift is $z = 2.741$ and that the strongest line is C IV rather than Lyα at $z = 3.76$. The tentative absorption trough blueward of C IV could indicate that this is a broad absorption line quasar. The spectrum is shown and discussed in § 4.

Only N2_64 does not show any reliable emission lines in either its optical or near-IR spectra. The optical spectrum does show weak continuum extending down to 3800 Å without a

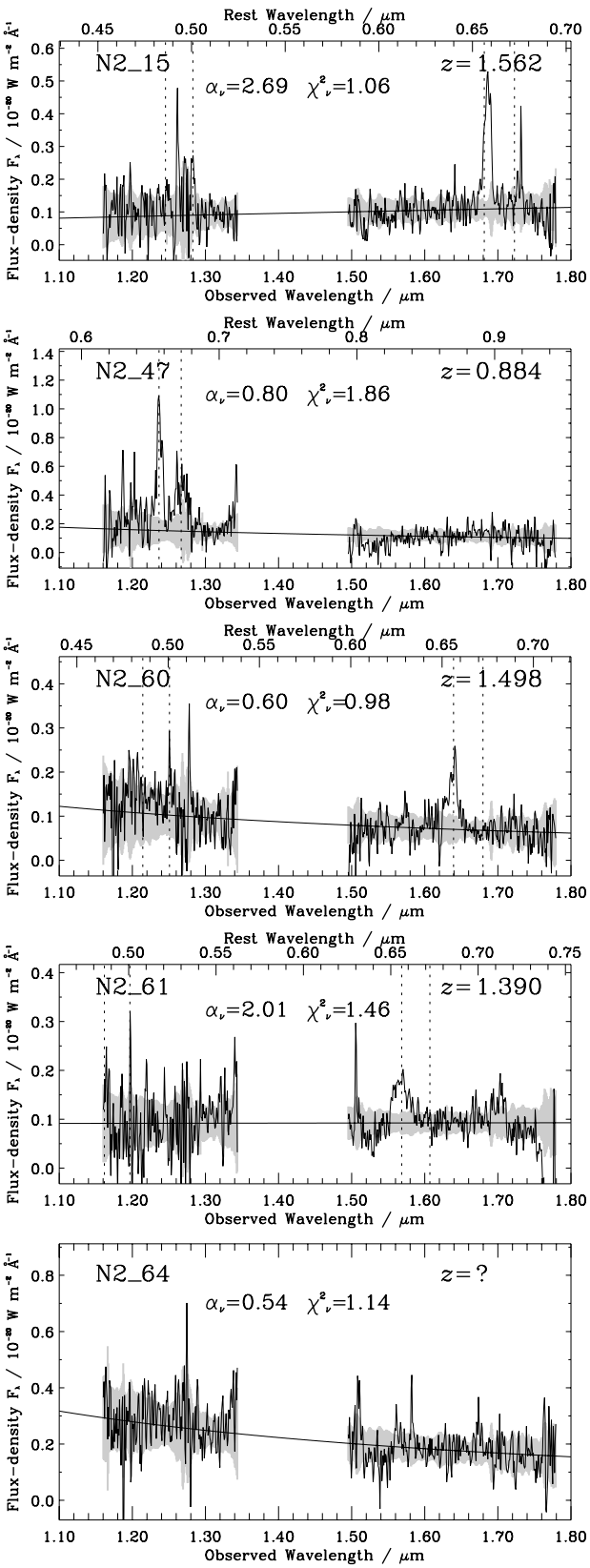

FIG. 3.—Near-infrared spectra of the five sources observed with the OHS. Vertical dotted lines mark the expected locations of the Hβ λ4861, [O III] λ5007, Hα λ6563, and [S II] λ6716/λ6731 emission lines. The curve is the best fit of a single power law to the continuum. The values of the slope α_ν and the goodness of fit χ^2_ν refer to this power-law fit. The gray shaded region is the ± 1 σ noise added to the best-fit power-law continuum. The gap in the spectra is due to the region between the *J* and *H* bands, which is heavily affected by atmospheric absorption.

break, suggesting a redshift of $z < 2.1$. We note that for redshifts in the ranges $1.0 < z < 1.3$ or $1.7 < z < 2.0$ the two strongest lines in the spectra of N2_15, N2_47, and N2_60 would not be observed in the wavelength range covered by the OHS spectra, so these are likely redshift ranges for N2_61. The lack of an Lyα emission line in the optical spectrum supports the $1.0 < z < 1.3$ range, but reddened quasars can have very weak Lyα lines as a result of resonant dust scattering (Charlot & Fall 1991) so the higher range is also possible. We have considered the possibility that N2_64 is a BL Lac object with optical and X-ray fluxes dominated by beamed synchrotron. However, this object is not detected in a very deep 1.4 GHz radio observation (rms 9 μJy; Ivison et al. 2002), which leads us to conclude that it is not a BL Lac object.

4. SPECTRAL FITTING

Single power-law continuum fits to the OHS spectra were attempted for all five quasars with near-IR spectra. Wavelength regions containing quasar emission lines were masked out and an iterative χ^2 fit was performed. The best-fit power-law slopes, α_ν, and the associated reduced χ^2, χ^2_ν, are labeled in Figure 3. The mean optical spectral index of radio-quiet quasars is $\alpha_\nu = 0.4$ (Brotherton et al. 2001). Two of the quasars, N2_15 and N2_61, have very steep spectra with $\alpha_\nu \geq 2$. The other three quasars have $0.5 < \alpha_\nu < 0.8$, which is slightly steeper than the mean spectral index but within the red tail of the distribution observed in optically selected samples such as the SDSS (Richards et al. 2003). For N2_15, N2_60, and N2_64 a power law provides a good description of the continuum shape ($\chi^2_\nu \approx 1$). N2_47 has $\chi^2_\nu \approx 2$ and shows deviations from a power law, particularly a dip at a rest-frame wavelength of $\approx$0.8 μm, which is also apparent in the SDSS composite quasar spectrum (Vanden Berk et al. 2001). Although for N2_61 the best fit has $\chi^2_\nu \approx 1.5$, the fitted slope of $\alpha_\nu = 2.01$ describes the overall continuum slope well.

Table 1 lists the optical *V*, *R*, *I*, and near-infrared *H* magnitudes of these quasars. At the redshifts of these quasars, the observed optical emission is probing the rest-frame ultraviolet. The colors of a typical unreddened quasar would be $V - I \approx 0.5$ and $V - H \approx 2$. It is clear from this table that the rest-frame UV and UV–optical colors of the quasars we have observed are considerably redder than those of a typical quasar.

The red colors of these quasars can be explained by an intrinsic shape similar to ordinary quasars that is reddened by a foreground screen of dust. There are other possible explanations for red quasars: (1) an optical synchrotron–dominated spectrum (e.g., Francis et al. 2001) and (2) a host galaxy–dominated spectrum (e.g., Vanden Berk et al. 2001). We discount the former possibility because optical synchrotron only dominates in powerful radio-loud quasars with flat radio spectra and the latter because our near-infrared observations show that these sources are unresolved in 0.″5 seeing.

To constrain the amount of reddening required to produce these red quasars, we have performed a fit to the optical photometry and near-infrared spectroscopy. The fact that our objects are spatially unresolved in both the optical and near-IR means that we can use a single-component quasar fit. For a typical quasar template we use the composite radio-quiet quasar spectrum from the FIRST Bright Quasar Survey (FBQS; Brotherton et al. 2001). We use this rather than the SDSS composite of Vanden Berk et al. (2001) because the

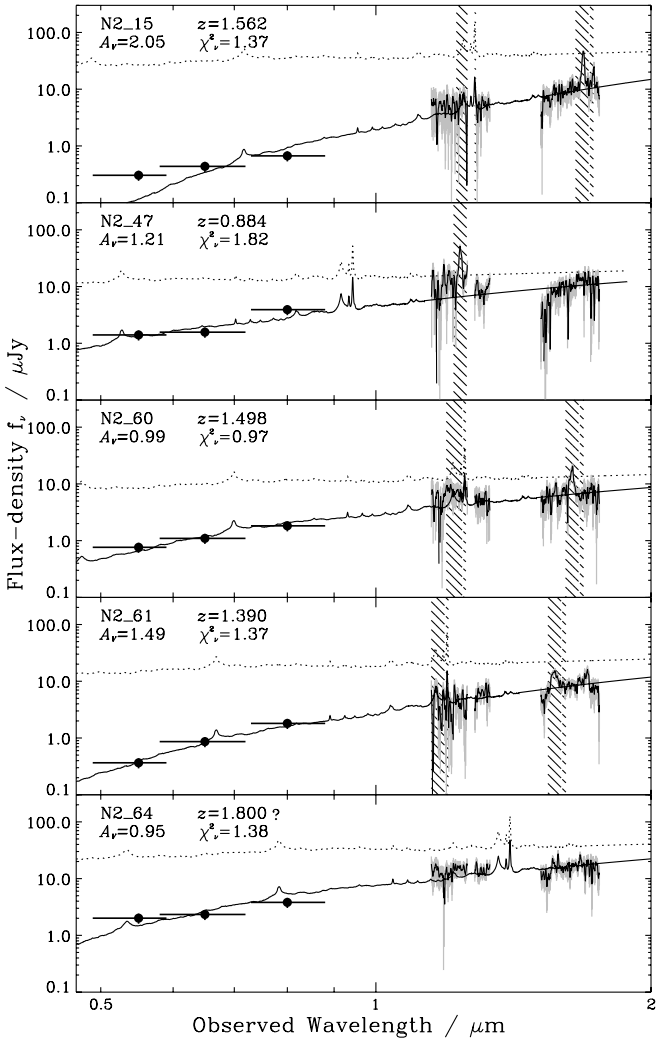

FIG. 4.—Observed-frame optical photometry and near-infrared spectra of the five reddened quasars observed with OHS. Near-IR spectroscopy is shown by the solid line surrounded by gray shading to indicate the ± 1 σ noise. Optical photometry in the V, R, and I bands is shown by filled circles at the effective wavelengths of the passbands with horizontal lines showing the extent of the passbands and a vertical line the photometric errors. The best-fit reddened composite quasar spectra are shown (assuming an SMC extinction law only). The values of the extinction A_V and the goodness of fit χ^2_ν refer to this fit. The dotted quasar spectrum is the intrinsic, unreddened spectrum. Regions of the near-IR spectra excluded from the fitting as a result of the presence of emission lines are hatched.

SDSS composite shows a break at greater than 4000 Å where contamination by host galaxy light becomes important. In contrast, the FBQS radio-quiet quasar composite spectrum shows a constant power law from the UV right out to 6000 Å. We extend the composite redward of 6000 Å by continuing the power-law slope of $\alpha_\nu = 0.43$. We do not add in emission lines such as Hα, since we will only be using the line-free regions of the quasar spectrum for continuum fitting. The composite quasar spectrum is then subjected to a variable amount of dust reddening, and an iterative χ^2 routine determines the best-fit amount of reddening. The routine allows for reddening with three different extinction laws: that of our Galaxy, the LMC, and the SMC, adopting the parametric extinction laws of Pei (1992).

The optical photometry and near-infrared spectroscopy for these five quasars are shown in Figure 4. Also plotted are the

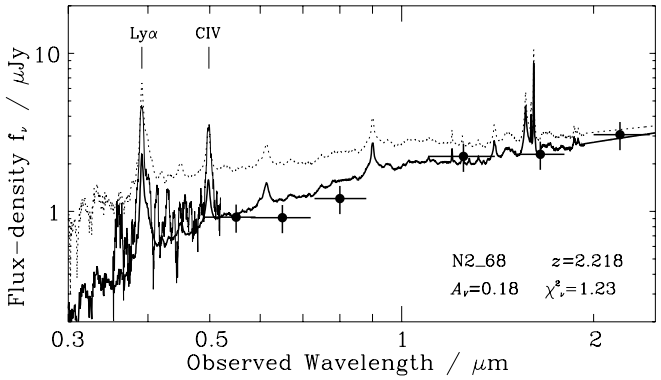

FIG. 5.—ISIS blue-arm optical spectrum (0.35–0.52 μm) and optical (V, R, I) and near-IR (J, H, K) photometry points for N2_68. The best-fit reddened composite quasar spectrum is shown by a thick line (assuming an SMC extinction law only). The dotted quasar spectrum is the intrinsic, unreddened spectrum. The best-fit quasar has a small amount of reddening ($A_V \approx 0.2$), but it is possible that the near-IR photometry is dominated by host galaxy light, in which case the optical data can be well fitted by a quasar with no reddening. Regions of the optical spectrum containing the Lyα and C IV emission lines and data shortward of Lyα are excluded from the fitting.

results of the reddened quasar fitting process: both the reddened spectrum and the original unreddened spectrum. This illustrates that none of the five quasars have optical and near-infrared spectra similar to the unreddened quasar template. It also shows that the observed flux in the optical has been heavily affected by absorption (by factors of 10–100). Although the fitting was performed for three different extinction laws, only the SMC extinction law is shown in this plot. The χ^2_ν values for the different extinction laws varied by less than 10% for most objects (the main exception being N2_15 where a Galactic extinction law fits the optical photometry much better and has a $\chi^2_\nu = 1.1$). The best-fit A_V values are systematically higher for LMC (120% of SMC) and Galactic (130% of SMC) type dust because of their lower ratios of UV to optical absorption. With the limited data available we are not able to draw any firm conclusions on which dust extinction law provides the best fit to these reddened quasars.

For N2_68, we do not have near-IR spectroscopy, but we do have an optical spectrum from the blue arm of ISIS at the WHT and optical (V, R, I) and near-IR (J, H, K) photometry. The S/N in the optical photometry is sufficient to tell that the source is spatially unresolved. However, the source is faint in the near-IR ($J = 22.14 \pm 0.11$, $H = 21.65 \pm 0.16$, $K = 20.83 \pm 0.18$), and it is not possible to tell if the near-IR emission is resolved or not. A passively evolving L_* galaxy formed in an instantaneous starburst at $z = 5$ has $K = 20.2$ at the redshift of N2_68, so it is certainly possible that the near-IR fluxes are dominated by extended, host galaxy emission. In Figure 5 we show the optical spectrum and photometry data for N2_68. We have performed reddened quasar fitting to these data in a manner similar to that described previously for the other EDXS quasars. We find that there is relatively little reddening for N2_68 ($A_V \approx 0.2$ for an SMC extinction law and $A_V \approx 0.4$ for a Milky Way law). If the near-IR fluxes are dominated by the host galaxy, then the data are consistent with an unreddened quasar.

N2_35 does not have near-IR spectroscopy but does have an optical spectrum described in § 3.3 and shown in Figure 6. This spectrum is used to fit the same range of reddened quasar models as detailed above. N2_35 is very faint in the near-IR and is undetected at the J and H bands. It is detected at K band

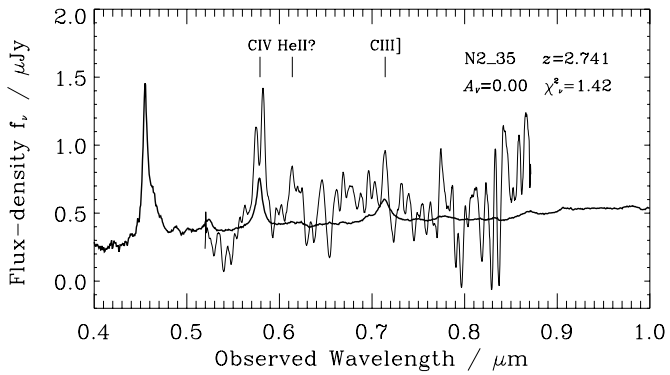

FIG. 6.—Gemini North GMOS optical spectrum (*thin line*) of N2_35. The best-fit composite quasar spectrum is shown by a thick line. The best-fit quasar has no reddening. Regions of the optical spectrum containing the labeled emission lines are excluded from the fitting.

with $K = 21.04 \pm 0.16$ and is clearly resolved in that image (0.″6 seeing). As mentioned in the preceding paragraph, this magnitude is consistent with that of a quasar host galaxy at this redshift. Therefore, the *K*-band photometry was not included in the quasar fitting algorithm. The optical spectrum appears to show no reddening. Note that the *quasar K*-band magnitude predicted by this fit is $K = 22.4$, which explains why the host galaxy outshines the quasar at *K*.

5. COMPARISON OF X-RAY AND OPTICAL ABSORPTION

For eight of the nine quasars in our optical magnitude-limited EDXS-N2 sample, we have constrained the amount of reddening of the optical quasar emission. The optical dust reddening $E(B-V)$ is calculated from the fitted A_V values assuming the standard values of $R_V = 3.1$ (Galactic) or $R_V = 2.9$ (SMC). We can determine the gaseous X-ray–absorbing column by using the observed *Chandra* hardness ratio and assuming an intrinsic power law with $\Gamma = 2$ as found by Mainieri et al. (2002). X-ray absorption in the hard, soft, and full bands is determined following the prescription of Morrison & McCammon (1983).

Figure 7 plots the optical reddening due to dust against the absorbing column due to gas for these quasars. The left panel shows the results of fits with Galactic dust, and the right panel is for SMC dust. Also shown are curves for a Galactic gas-to-dust ratio [$N_{\rm H} = 5.8 \times 10^{21} E(B-V)$; Bohlin et al. 1978] and an SMC gas-to-dust ratio [$N_{\rm H} = 5.2 \times 10^{22} E(B-V)$; Bouchet et al. 1985]. The factor of 10 difference between these is attributed to the lower metallicity in the SMC meaning less metals available for dust formation.

The EDXS quasars tend to have higher gas-to-dust absorption ratios than Galactic, although some of them are quite close to the curve and do not show a statistically significant deviation from the Galactic value. In contrast, the quasars are evenly distributed around the SMC gas-to-dust ratio. Note that sources with $E(B-V) > 1$ are not likely to be in our sample because their rest-frame UV emission may be too highly obscured for them to pass the $R < 25$ mag limit and/or the host galaxy may dominate, giving an extended appearance. Similarly, there are many quasars with $E(B-V) < 0.3$ that have $R < 23$ and were therefore not followed up in this paper (I. Pérez-Fournon et al. 2004, in preparation). Hence, this diagram should be interpreted as the gas column densities of a nearly complete sample of lightly reddened quasars.

The discovery of N2_25 with a gas-to-dust absorption ratio 100 times Galactic (Willott et al. 2003) along with other reports of high gas-to-dust ratio in the literature were the motivation for this study. The only other quasar with such an extreme ratio is N2_35. This quasar appears to be completely unobscured in the optical but has a very hard X-ray spectrum. The optical spectrum shows hints that this is a broad absorption line quasar: these quasars are known to have hard X-ray spectra due to a large column density (Gallagher et al. 2002) but comparatively

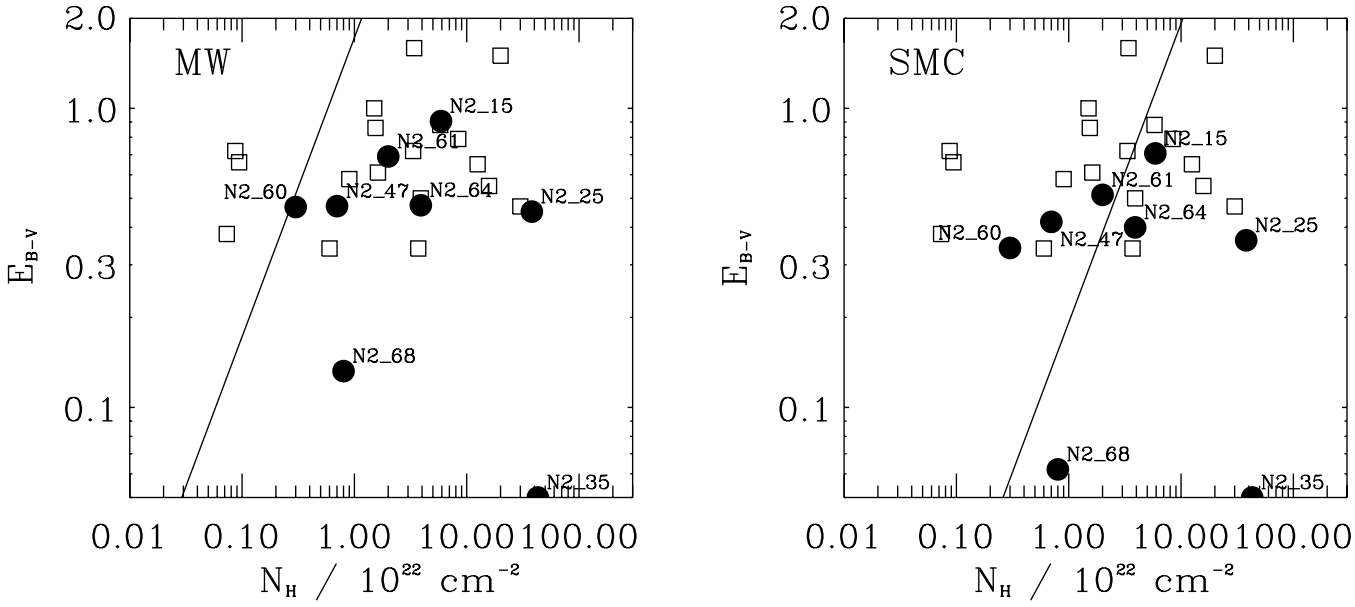

FIG. 7.—Comparison of the optical reddening due to dust $E(B-V)$ and gas absorption column density $N_{\rm H}$ for the optically faint EDXS-N2 quasars (*circles*). *Left*: Dust extinction values plotted on this panel are for the fits with a Milky Way extinction law. The curve shows the standard Galactic ratio. Also plotted are the Seyfert galaxies studied by Maiolino et al. (2001b; *open squares*). *Right*: Dust extinction values plotted here are for the fits with an SMC extinction law, and the curve shows the gas-to-dust ratio for the SMC. The Seyfert data are plotted in this panel with the same values of $E(B-V)$ as for the Milky Way, since the reddening was derived from observations at wavelengths greater than 4000 Å where the two extinction curves are the same. N2_35 shows no measurable optical extinction but is plotted at the minimum $E(B-V)$ on these plots.

little optical reddening (Reichard et al. 2003). Apart from these two quasars with extreme gas-to-dust absorption ratios, a ratio in the range 1–10 times Galactic is typical of the rest of the sample.

Maiolino et al. (2001b) compared the gas and dust absorption properties of a sample of nearby Seyfert galaxies and found that they typically have higher ratios than Galactic. The data from this study are also plotted in Figure 7. The Seyfert galaxies and EDXS quasars tend to occupy similar locations in this plot, suggesting that higher gas-to-dust absorption ratios in AGNs are not a strong function of luminosity and/or redshift. One should note that the particular selection criteria used by Maiolino et al. (2001b) for their Seyfert sample almost inevitably led to the sample being dominated by objects with high gas-to-dust absorption ratios and the effect of any such biases should become clearer with a volume-limited Seyfert sample being studied with *XMM-Newton* (Cappi 2004).

The similarity of the gas-to-dust ratios in AGNs and the SMC is not easily explained. In the case of the SMC, the gas-to-dust ratio is about 10 times higher than that of the galaxy because its metallicity is about 10 times lower (Bouchet et al. 1985). In the case of AGNs, supersolar metallicities are common in the circumnuclear region (Hamann & Ferland 1999). In any case, metallicity effects are not so important when the gas-absorbing column density comes from an X-ray measurement (Maiolino et al. 2001a). This is because the measured X-ray absorption is due to photoelectric absorption by metals, so the derived gas density is proportional to the metallicity. Given the quite different physical conditions in AGN environments and in the SMC, the similarity of these gas-to-dust ratios is likely just a coincidence.

There are three basic ways to interpret the higher gas-to-dust absorption ratios in the AGN environment as compared to the Milky Way: (1) the dust grain composition is different so dust is less effective at absorbing UV radiation; (2) the majority of the X-ray absorption occurs close to the ionizing radiation source, within the dust sublimation radius; and (3) the ratio of gas to dust is higher than in our Galaxy. These possibilities are discussed in more detail in Maiolino et al. (2001a, 2001b), and work still needs to be done to determine which effect is dominant.

We now return to the issue of the effect that obscuration has on the observed optical–to–X-ray flux ratio. The bottom panel of Figure 2 and the statistics presented in § 2.2 showed that as the X-ray emission from quasars gets more heavily obscured, the ratio of optical to X-ray flux decreases. Can this obscuration be simply explained by an absorber composed of dust and gas? To test this, we have simulated the effects of gas and dust on the optical and X-ray flux of quasars at various redshifts. The intrinsic X-ray slopes of the quasars are modeled with a $\Gamma = 2$ power law. The same procedure as detailed above was used to relate $N_{\rm H}$, HR, and the amount of full-band X-ray absorption. The optical absorption in the observed-frame R band was calculated by assuming the relevant extinction curve of Pei (1992). Again, we consider both the Milky Way and SMC extinction laws and their gas-to-dust ratios. We now replot the data from Figure 2 on Figure 8 adding in curves that show how the optical–to–X-ray flux ratio and hardness change as one increases the column of absorbing material. We plot Galactic and SMC curves for four different redshifts. Since the optical flux is much more readily depressed than the full-band X-ray flux for typical gas-to-dust ratios, the optical–to–X-ray flux ratio decreases as the absorbing column is increased (except for small columns at $z = 0$ for the SMC). The strong

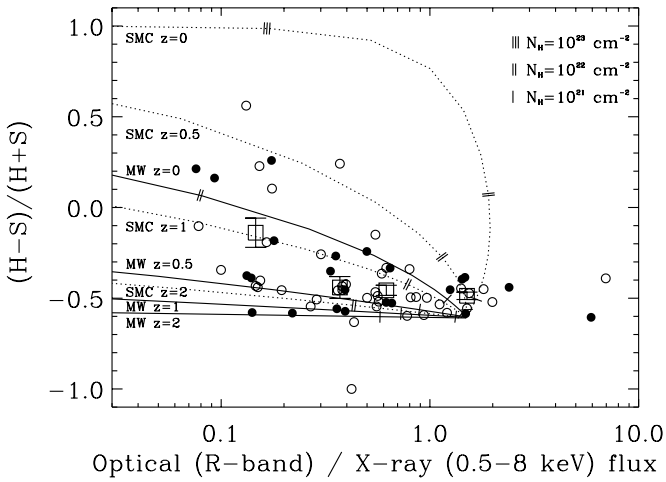

FIG. 8.—Same data as plotted in bottom panel of Fig. 2. The curves show how the observed hardness ratio of a quasar with intrinsic optical–to–X-ray flux ratio of 1.5 and X-ray power law of slope $\Gamma = 2.0$ would depend on the observed optical–to–X-ray flux ratio for a range of obscuring gas and dust properties at various redshifts. At each of the four plotted redshifts a curve is shown for Milky Way (*solid line*) and SMC (*dotted line*) dust (and the associated gas-to-dust ratio) as described in § 5. Each curve corresponds to a range of absorbing columns that are indicated by tick marks along these curves.

redshift dependence of these curves is due to the fact that the k-corrections for obscured AGNs in the optical/UV and X-rays have opposite trends.

Figure 8 shows that if the quasars were to lie mostly in the redshift range $0 < z < 0.5$, then their range of hardness ratio and optical–to–X-ray ratio could be explained by a small intrinsic scatter coupled with absorption by gas and dust with Galactic properties. However, very few of these quasars lie at such low redshifts, and spectroscopy (§ 3; Barger et al. 2002) shows that most of them lie within the redshift range $1 < z < 2.5$. At these redshifts, simple Galactic gas and dust obscuration cannot simultaneously explain the hardness ratios and optical–to–X-ray ratios. In comparison, the curves for the SMC provide a much better match to the data. This is mostly due to the 10 times higher gas-to-dust ratio and not differences in the dust extinction laws.

In Willott et al. (2003) we speculated that if there are a large fraction of AGNs that are type 1 in the optical (i.e., broad permitted lines) and type 2 in the X-ray (hard X-ray spectrum due to absorption), then they could be a major contributor to the hard X-ray background. This would lessen the need for optically obscured sources to dominate the hard X-ray background. We can obtain an estimate of the contribution of such sources to the X-ray background from the number of sources with unresolved optical counterparts and high hardness ratios. From consideration of the hardness ratios and Figure 7 we specify sources with HR > -0.2 as hard enough to be type 2 in the X-ray. This corresponds to an absorption column density of 3×10^{22} cm^{-2} at $z = 2$ assuming an intrinsic $\Gamma = 2$ power law. In the EDXS-N2 region there are four sources (N2_15, N2_25, N2_35, and N2_37) that have HR > -0.2 and are optically unresolved. This is out of a parent sample of 61 sources above the flux limit of greater than 2×10^{-15} ergs cm^{-2} s^{-1} and with S/N greater than 5 σ, giving 6% of the sample. A similar analysis in the CDF-N also finds that 6% of the sources have HR > -0.2 and are optically unresolved. Since the sources in these samples are in the flux range that dominates the hard X-ray background (50%–64% of the

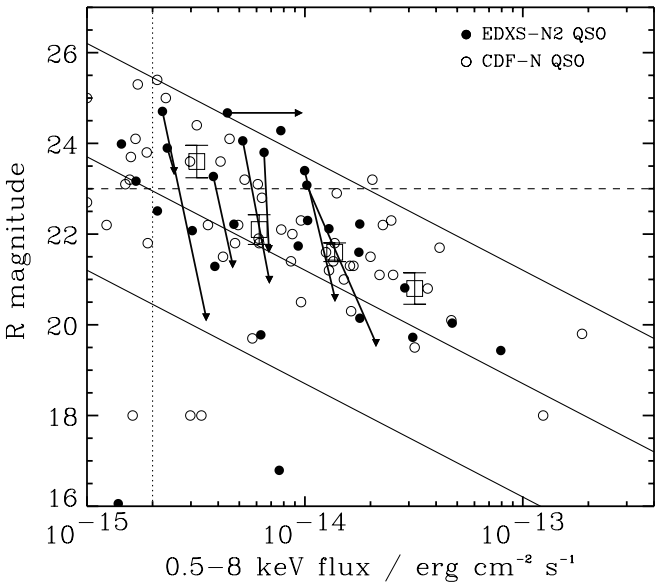

FIG. 9.—As in Fig. 1, the *R* magnitudes of EDXS-N2 (*filled circles*) and CDF-N (*open circles*) quasars are plotted against full-band X-ray flux. The squares with error bars are the median *R* magnitude against median X-ray flux as in Fig. 1. The arrows show the deabsorbed *R* magnitudes and X-ray fluxes of the EDXS-N2 quasars with $R > 23$ for which the optical reddening has been determined. The dereddened *R* magnitudes of these optically faint quasars bring them back into the typical range of optical–to–X-ray flux ratio.

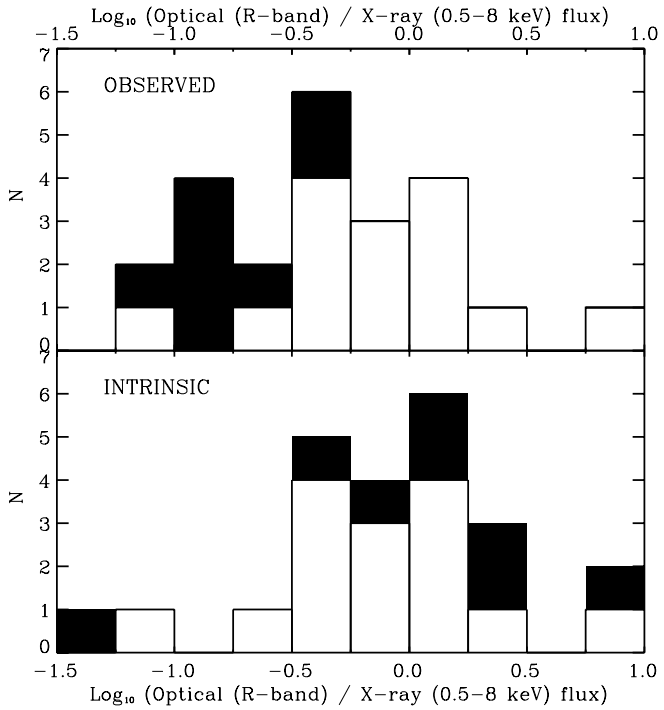

FIG. 10.—Histogram of optical–to–X-ray flux ratio for EDXS-N2 quasars. The top panel shows the histogram of ratios as observed. The black filled histogram shows the eight sources for which the optical reddening has been determined. In the bottom panel the absorption-corrected optical–to–X-ray flux ratios for these eight sources are shown in black. The effect of these corrections is to shift the histogram to higher optical–to–X-ray flux ratios.

2–8 keV background is resolved by the EDXS; Manners et al. 2003), we conclude that only about 6% of the sources responsible for the 2–8 keV X-ray background appear as type 1 in the optical and type 2 in the X-ray.

6. EFFECT OF OBSCURATION ON OBSERVED OPTICAL–TO–X-RAY RATIO

Having shown that obscuration plays an important role in the observed properties of type 1 AGNs, we now revisit the effect this may have on the observed optical–to–X-ray ratio. Given the fact that at the redshifts where most quasars are observed ($z > 1$) the optical–to–X-ray ratio is so strongly dependent on the obscuration, this may skew the observed distribution of optical–to–X-ray ratios away from their intrinsic values.

Figure 9 plots optical magnitude against full-band X-ray flux for quasars from the EDXS-N2 and CDF-N surveys. For eight of the nine EDXS-N2 quasars with observed magnitudes $R > 23$ we have determined the optical reddening and X-ray absorption. We use here the reddening values determined with the SMC extinction law but note that they are very similar to those determined with the Milky Way law. Plotted in Figure 9 are arrows showing the locations of these quasars once they have been deabsorbed in the optical and X-ray. The effect of absorption is quite dramatic, particularly at optical wavelengths. This illustrates that these quasars that are observed to be optically faint are mostly not intrinsically optically faint. The main exception is N2_35, which does not show any optical absorption but is heavily obscured in the X-rays and hence deabsorbing it actually decreases the optical–to–X-ray flux ratio.

To determine how big an effect this has on the whole population of quasars, in Figure 10 we show a histogram of the optical–to–X-ray flux ratio for all the EDXS-N2 quasars with 0.5–8 keV fluxes greater than 2×10^{-15} ergs cm^{-2} s^{-1}. The top panel shows the observed optical–to–X-ray flux ratios. The bottom panel shows the intrinsic ratios for the sources shown with deabsorbing arrows in Figure 9. Note that the absorption-corrected histogram could be incomplete for two reasons. First, there may be quasars with $R > 25$ and low values of optical–to–X-ray flux ratio that are not identified as such because of the limited depth and resolution of the optical imaging. Second, some of the quasars with $R < 23$ will be subject to obscuration, and correcting for this would likely shift their optical–to–X-ray flux ratios to higher values. Despite these incompletenesses, this plot clearly shows that the typical intrinsic value of the optical–to–X-ray flux ratio is greater in all but one case (N2_35, the possible broad absorption line quasar) than one would think from looking at the raw data.

The ratio of optical and X-ray flux is often expressed in terms of the optical–to–X-ray spectral index, α_{ox}, where

$$\alpha_{ox} = \frac{\log(f_{2\,\mathrm{keV}}/f_{2500\,\text{Å}})}{\log(\nu_{2\,\mathrm{keV}}/\nu_{2500\,\text{Å}})}. \quad (1)$$

The α_{ox} distribution for bright, low-redshift optically selected quasars comprises a roughly Gaussian distribution with a peak at $\alpha_{ox} = -1.5$ and a tail of about 10% of the quasars at $\alpha_{ox} < -2$ (Brandt et al. 2000; Vignali et al. 2003). The existence of broad or associated absorption lines in most of these $\alpha_{ox} < -2$ quasars suggests that soft X-ray absorption is the reason for the higher optical–to–X-ray flux ratios in these quasars. Anderson et al. (2003) have recently confirmed that there is a weak anticorrelation between optical luminosity and α_{ox} and showed that for moderate-luminosity X-ray–selected quasars a typical value of α_{ox} is -1.4.

Two of the quasars in the EDXS-N2 sample (N2_25 and N2_35) are absorbed by columns greater than 10^{23} cm^{-2}. For these quasars, the rest-frame 2 keV is below the photoelectric

cutoff, leading to almost total absorption of the 2 keV flux. The calculated observed α_{ox} values for these quasars assuming an X-ray spectrum with absorption columns implied by the hardness ratios are -3.3 and -4.2, respectively. Applying corrections for the obscuration in the X-rays and optical (for N2_25 only, since N2_35 is optically unobscured) leads to intrinsic values of $\alpha_{ox} = -1.0$ and -1.2, respectively. The quasar N2_68, which shows little or no reddening or X-ray absorption, has $\alpha_{ox} = -1.6$.

For the other five EDXS-N2 quasars discussed in this paper the observed optical–to–X-ray spectral indices lie in the small range $-1.3 < \alpha_{ox} < -1.0$. After corrections for optical and X-ray absorption, these spectral indices all get steeper and lie in the range $-1.3 < \alpha_{ox} < -1.6$, which is typical of lower redshift quasars with similar optical luminosities (Anderson et al. 2003). This is interesting because the behavior for high-redshift, X-ray–selected quasars contrasts with that for low-redshift, optically selected quasars. In the optically selected sample the obscuration is strongest at X-ray energies, since strong reddening of the optical continuum would push the optical magnitude above the magnitude limit. In the X-ray–selected sample the obscuration is strongest in the (observed frame) optical. Note that the faint optical and X-ray flux limits in our survey are such that a much more representative range of absorbed quasars is present than in samples with brighter flux limits.

Risaliti et al. (2001) showed that optical emission line–selected quasars tend to have steeper α_{ox} than optical color–selected quasars. They interpret this as being due to a larger amount of X-ray absorption in the slightly reddened quasars and suggest that this shows that a large population of quasars exist that are type 1 in the optical and type 2 in the X-rays. This behavior is seen for N2_25 and N2_35 but not for the rest of our sample. As discussed in § 5, we find that such quasars can only contribute a small fraction of the X-ray background. The differences between our findings and those of Risaliti et al. (2001) are likely due to two issues: (1) their definition of the X-ray flux was based on soft X-rays (*ROSAT* PSPC counts) that are more readily absorbed than the *Chandra* full-band flux, and (2) their emission-line–selected quasars have a very bright optical magnitude limit unlike ours, which are X-ray selected with faint optical magnitudes.

Under the assumption that most of the optically bright ($R < 23$) EDXS-N2 quasars have little or no reddening, their intrinsic α_{ox} values are similar to the absorption-corrected values we have found. Thus, the intrinsic spread in α_{ox} is much narrower than the observed range. This is very important for constraining the optical and X-ray radiation production mechanisms. Since the EDXS-N2 sample does not yet have complete redshift and reddening information, an examination of the intrinsic spread in α_{ox} is beyond the scope of the current paper but is clearly an important goal for the future.

7. CONCLUSIONS

Deep X-ray surveys are capable of uncovering the AGNs responsible for most of the supermassive black hole accretion history of the universe. Combined X-ray and optical/near-infrared observations of lightly reddened quasars from such X-ray surveys are a powerful probe of the physical conditions of the obscuring material. We have used optical and near-infrared photometry and spectroscopy to constrain the amount of reddening in the light from optically faint quasars. Our main conclusions are as follows:

1. Optically faint ($R > 23$) quasars at $f_{0.5-8} > 2 \times 10^{-15}$ ergs cm^{-2} s^{-1} are mostly faint as a result of obscuration. Dereddening the observed R-band fluxes of these quasars gives them optical magnitudes similar to other quasars with these X-ray fluxes ($20 < R < 22$).
2. Assuming that most of the spread in X-ray hardness ratios is due to absorption by gas, we find that gas-to-dust ratios in reddened X-ray–selected quasars are typically a few times greater than the gas-to-dust ratio in the Milky Way and similar to those in Seyfert galaxies.
3. The fraction of quasars responsible for the X-ray background that are type 1 in the optical (broad permitted lines) and type 2 in the X-ray (hard X-ray spectrum due to absorption) is only about 6%.
4. The observed distribution of optical–to–X-ray flux ratios of quasars at $z > 1$ is skewed to low values compared to the intrinsic distribution as a result of the fact that the observed-frame R-band light is emitted in the UV and is more easily obscured than the hard X-rays sampled by *Chandra*.

We thank the anonymous referee for comments that improved this paper. This work is based on data collected at Subaru Telescope, which is operated by the National Astronomical Observatory of Japan, and also on observations obtained at the Gemini Observatory, which is operated by the Association of Universities for Research in Astronomy, Inc., under a cooperative agreement with the NSF on behalf of the Gemini partnership: the National Science Foundation (United States), the Particle Physics and Astronomy Research Council (United Kingdom), the National Research Council (Canada), CONICYT (Chile), the Australian Research Council (Australia), CNPq (Brazil), and CONICET (Argentina). The William Herschel Telescope is operated on the island of La Palma by the Isaac Newton Group in the Spanish Observatorio del Roque de los Muchachos of the Instituto de Astrofisica de Canarias. Thanks to Steve Rawlings for assistance with some of the optical spectroscopy. C. J. W. thanks the NRC for support. C. S. acknowledges the award of a PPARC Advanced Fellowship.

REFERENCES

Abraham, R. G., et al. 2004, AJ, 127, 2455
Akiyama, M., et al. 2000, ApJ, 532, 700
Almaini, O., Boyle, B. J., Griffiths, R. E., Shanks, T., Stewart, G. C., & Georgantopoulos, I. 1995, MNRAS, 277, L31
Anderson, S. F., et al. 2003, AJ, 126, 2209
Barger, A. J., et al. 2002, AJ, 124, 1839
Bohlin, R. C., Savage, B. D., & Drake, J. F. 1978, ApJ, 224, 132
Bouchet, P., Lequeux, J., Maurice, E., Prevot, L., & Prevot-Burnichon, M. L. 1985, A&A, 149, 330
Brandt, W. N., Laor, A., & Wills, B. J. 2000, ApJ, 528, 637
Brandt, W. N., et al. 2001, AJ, 122, 2810
Brotherton, M. S., Tran, H. D., Becker, R. H., Gregg, M. D., Laurent-Muehleisen, S. A., & White, R. L. 2001, ApJ, 546, 775
Cappi, M. 2004, in Carnegie Observatories Astrophysics Series, Vol. 1: Coevolution of Black Holes and Galaxies, ed. L. C. Ho (Pasadena: Carnegie Obs.), 6
Charlot, S., & Fall, S. M. 1991, ApJ, 378, 471
Comastri, A., Setti, G., Zamorani, G., & Hasinger, G. 1995, A&A, 296, 1
Crawford, C. S., Gandhi, P., Fabian, A. C., Wilman, R. J., Johnstone, R. M., Barger, A. J., & Cowie, L. L. 2002, MNRAS, 333, 809

Fabian, A. C., Wilman, R. J., & Crawford, C. S. 2002, MNRAS, 329, L18
Francis, P. J., Drake, C. L., Whiting, M. T., Drinkwater, M. J., & Webster, R. L. 2001, Publ. Astron. Soc. Australia, 18, 221
Gallagher, S. C., Brandt, W. N., Chartas, G., & Garmire, G. P. 2002, ApJ, 567, 37
Hamann, F., & Ferland, G. 1999, ARA&A, 37, 487
Hasinger, G., et al. 2001, A&A, 365, L45
———. 2003, in AIP Conf. Proc. 666, The Emergence of Cosmic Structure, ed. S. Holt & C. Reynolds (New York: AIP), 227
Hornschemeier, A. E., et al. 2001, ApJ, 554, 742
Ivison, R. J., et al. 2002, MNRAS, 337, 1
Iwamuro, F., Motohara, K., Maihara, T., Hata, R., & Harashima, T. 2001, PASJ, 53, 355
Macklin, J. T. 1982, MNRAS, 199, 1119
Mainieri, V., Bergeron, J., Hasinger, G., Lehmann, I., Rosati, P., Schmidt, M., Szokoly, G., & Della Ceca, R. 2002, A&A, 393, 425
Maiolino, R., Marconi, A., & Oliva, E. 2001a, A&A, 365, 37
Maiolino, R., Marconi, A., Salvati, M., Risaliti, G., Severgnini, P., Oliva, E., La Franca, F., & Vanzi, L. 2001b, A&A, 365, 28
Manners, J. C., et al. 2003, MNRAS, 343, 293
McIntosh, D. H., Rix, H.-W., Rieke, M. J., & Foltz, C. B. 1999, ApJ, 517, L73
Morrison, R., & McCammon, D. 1983, ApJ, 270, 119
Mushotzky, R. F., Done, C., & Pounds, K. A. 1993, ARA&A, 31, 717
Norman, C., et al. 2002, ApJ, 571, 218
Oliver, S., et al. 2000, MNRAS, 316, 749
Pei, Y. C. 1992, ApJ, 395, 130
Reichard, T. A., et al. 2003, AJ, 126, 2594
Richards, G. T., et al. 2003, AJ, 126, 1131
Risaliti, G., Marconi, A., Maiolino, R., Salvati, M., & Severgnini, P. 2001, A&A, 371, 37
Roche, N. D., Almaini, O., Dunlop, J. S., Ivison, R. J., & Willott, C. J. 2002, MNRAS, 337, 1282
Schmidt, M., et al. 1998, A&A, 329, 495
Simpson, C. 1998, ApJ, 509, 653
Simpson, C., Dunlop, J. S., Eales, S. A., Ivison, R. J., Scott, S. E., Lilly, S. J., & Webb, T. M. A. 2004, MNRAS, submitted
Simpson, C., Rawlings, S., & Lacy, M. 1999, MNRAS, 306, 828
Steffen, A. T., Barger, A. J., Cowie, L. L., Mushotzky, R. F., & Yang, Y. 2003, ApJ, 596, L23
Stern, D., et al. 2002, ApJ, 568, 71
Szokoly, G. P., et al. 2004, ApJS, submitted (astro-ph/0312324)
Tozzi, P., et al. 2001, ApJ, 562, 42
Ueda, Y., Akiyama, M., Ohta, K., & Miyaji, T. 2003, ApJ, 598, 886
Vanden Berk, D. E., et al. 2001, AJ, 122, 549
Vignali, C., et al. 2003, AJ, 125, 2876
Watanabe, C., Ohta, K., Akiyama, M., & Ueda, Y. 2004, ApJ, 610, 128
Willott, C. J., Rawlings, S., Blundell, K. M., & Lacy, M. 2000, MNRAS, 316, 449
Willott, C. J., et al. 2003, MNRAS, 339, 397